

Supplementary Information for

Synthesis of Gold Nano-Mushrooms via Solvent- Controlled Galvanic Replacement to Enhance Phototherapeutic Efficiency

*Seounghun Kang^{b†}, Namgook Kwon^{a†}, Kyunglee Kang^a, Hojung Ahn^a, Sunbum Kwon^d, Dal-
Hee Min^{b,c*} and Hongje Jang^{a*}*

^a Department of Chemistry, Kwangwoon University, 20 Gwangwoon-ro, Nowon-gu, Seoul 01897, Republic of Korea

^b Department of Chemistry, Seoul National University, Seoul 08826, Republic of Korea

^c Institute of Biotherapeutics Convergence Technology, Lemonex Inc., Seoul 08826, Republic of Korea

^d Department of Chemistry, Chung-Ang University, Seoul 06974, Republic of Korea

Supporting data.

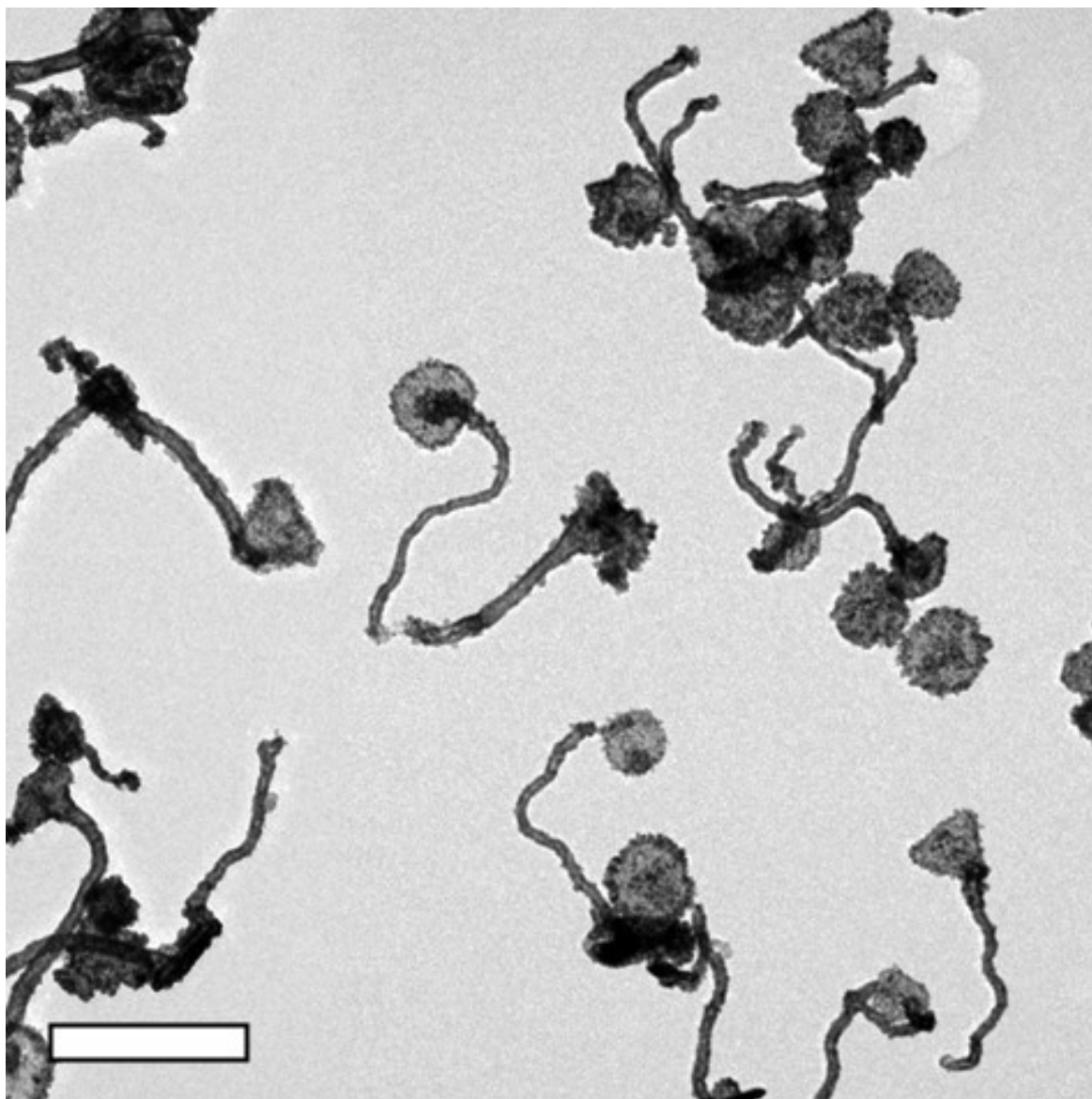


Figure S1. TEM image of mAuNPs. The scale bar is 200 nm.

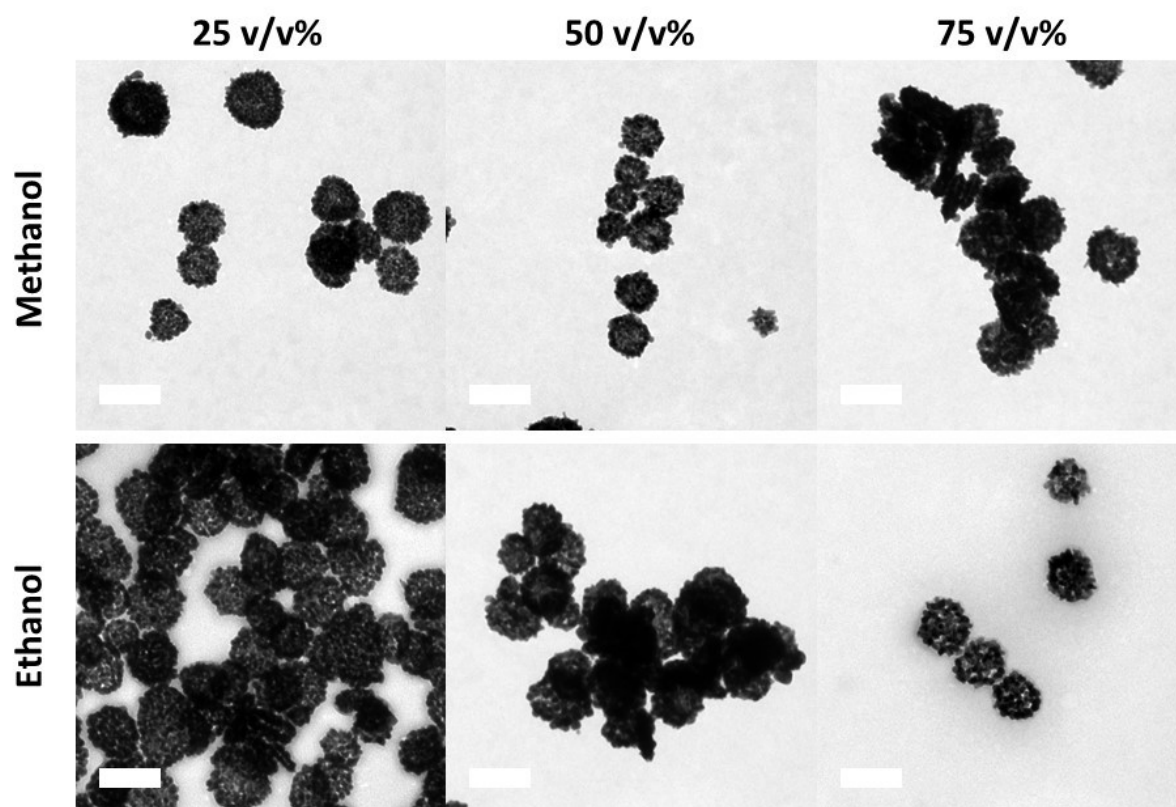


Figure S2. TEM image of SCGR of Ag nanoplates against methanol and ethanol. The scale bars are 100 nm.

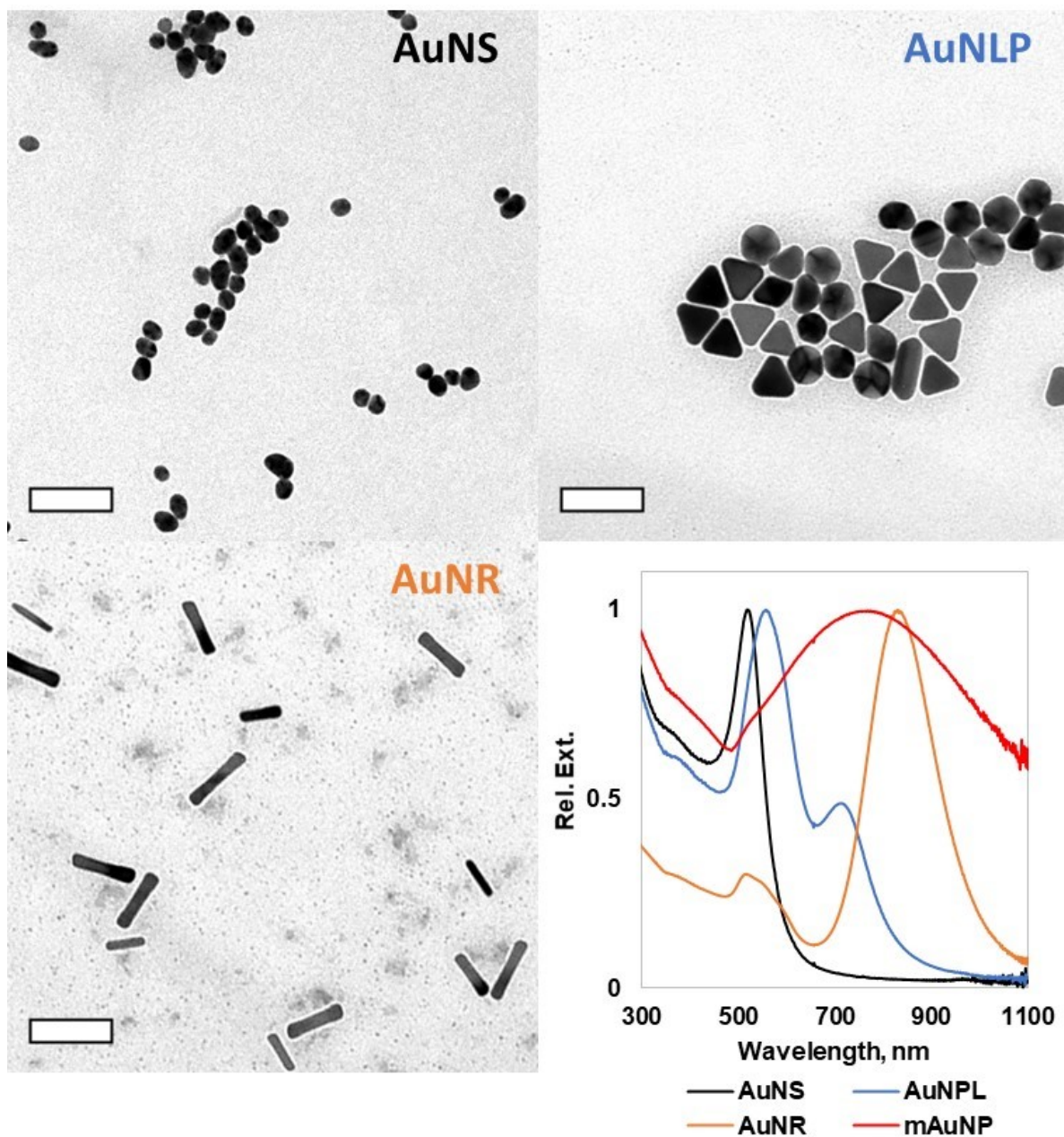


Figure S3. Various shaped Au nanoparticles for PT efficiency comparison with mAuNP. TEM images and UV-Vis spectra of AuNS, AuNPL, and AuNR showed morphology driven distinctive characteristics by localized surface plasmonic resonance. The scale bar is 100 nm.

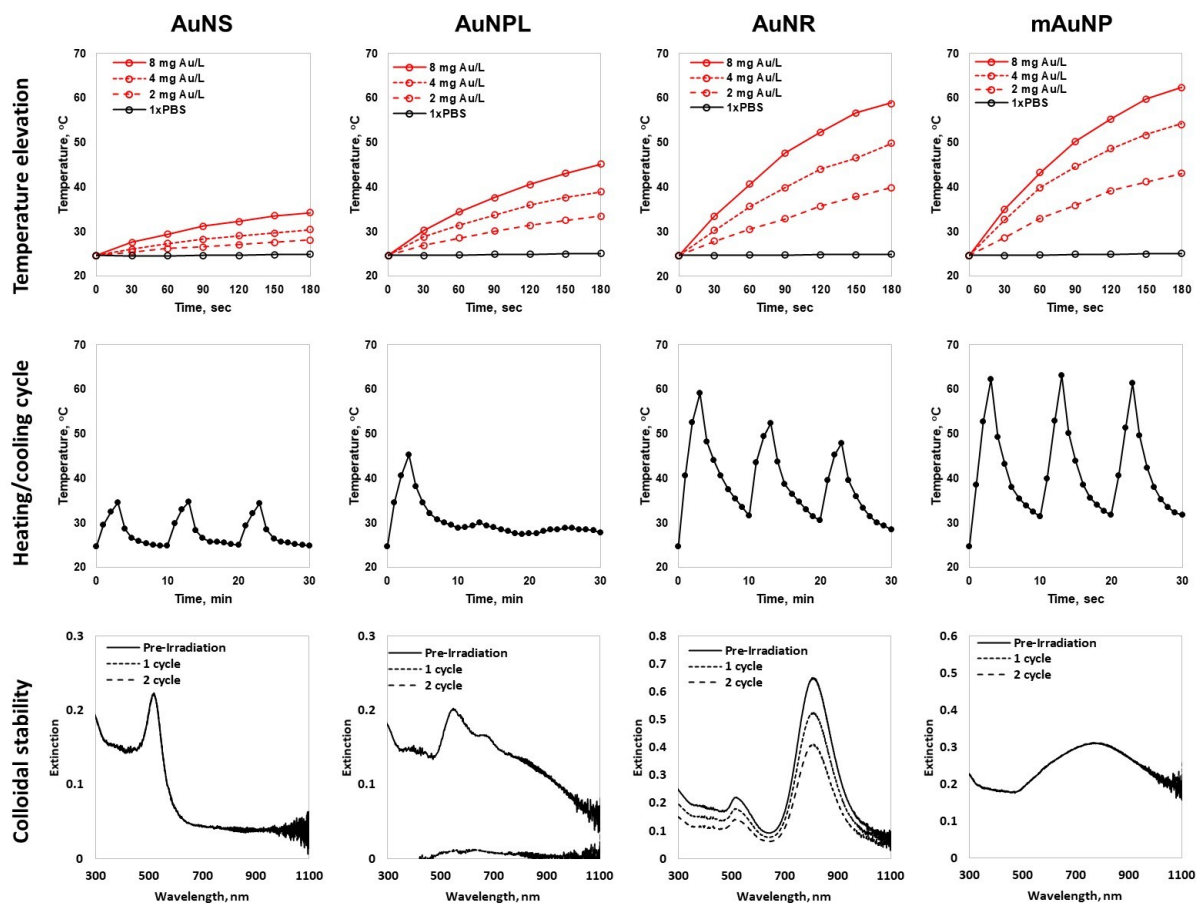


Figure S4. Photothermal conversion efficiency comparison between various shaped Au nanoparticles.

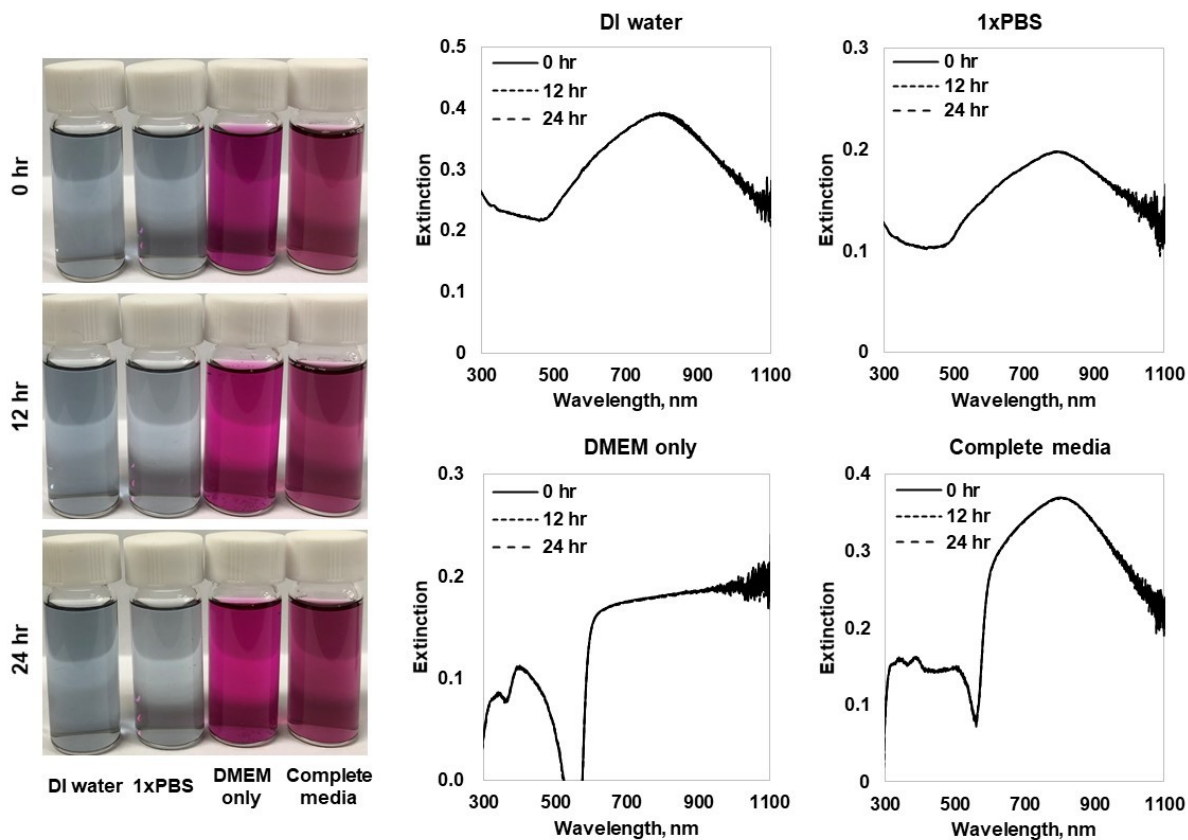


Figure S5. Colloidal stability of mAuNPs against various solvent conditions. According to the digital photograph images (left) and UV-Vis spectra (right), mAuNPs exhibited excellent stability during 24 h of incubation.

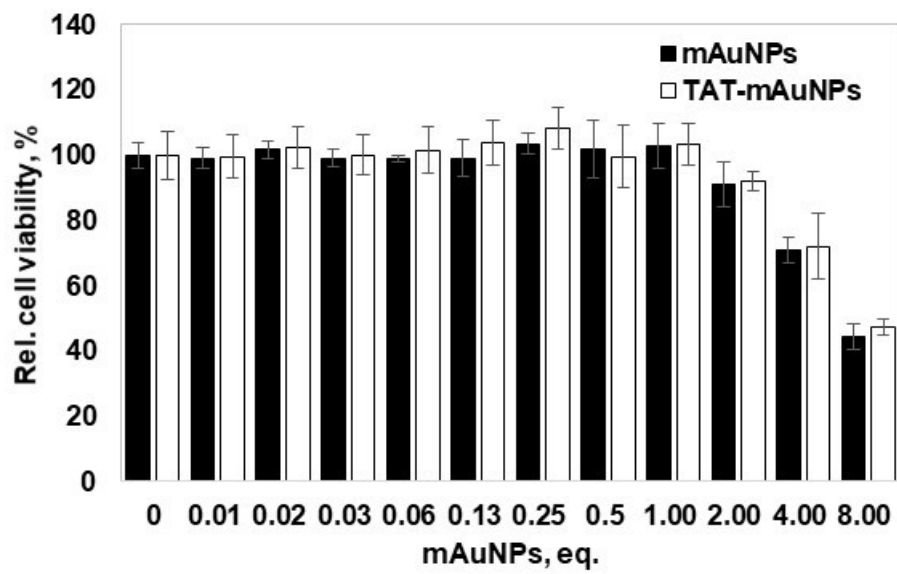


Figure S6. Cell viability assay for mAuNPs and TAT-mAuNPs against NS3 replicon Huh7 cells.

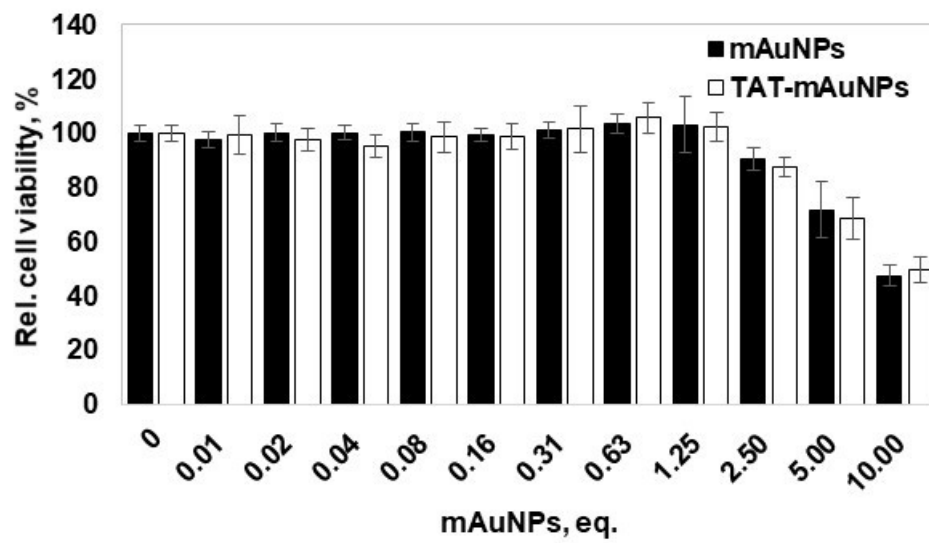


Figure S7. Cell viability assay for mAuNPs and TAT-mAuNPs against non-tumorigenic epithelial cell line, MCF-10A.

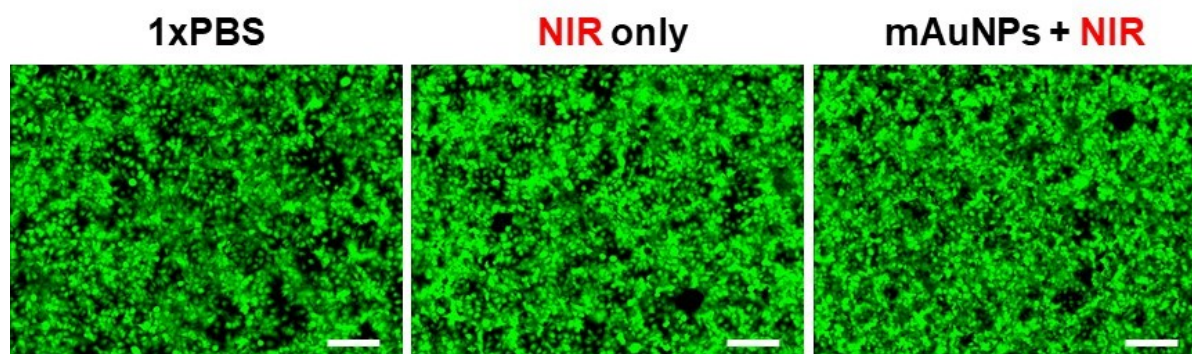


Figure S8. Fluorescence microscope image of NS3 replicon Huh7 cells. According to the live/dead staining, only NIR and mAuNPs with NIR irradiation conditions without TAT modification did not induced any cell apoptosis. The scale bar is 250 μm .

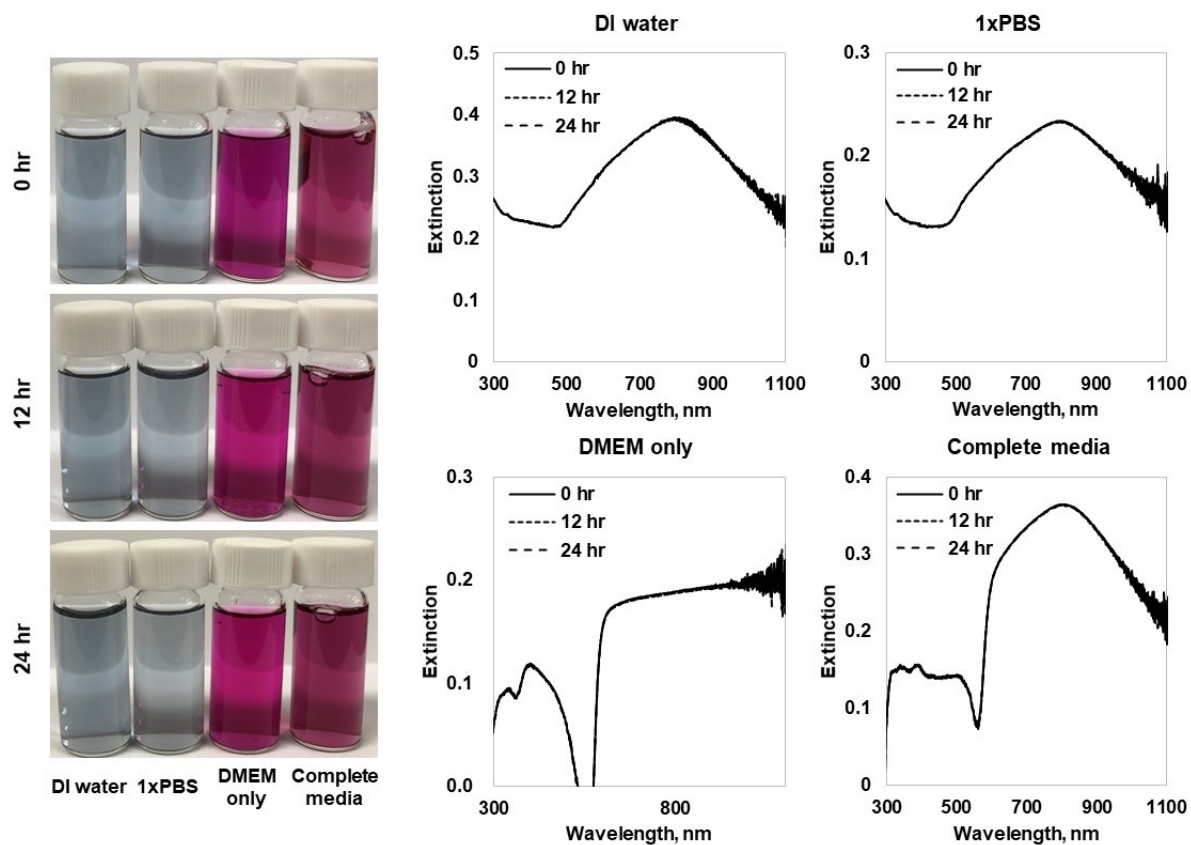


Figure S9. Colloidal stability of TAT-mAuNPs against various solvent conditions. According to the digital photograph images (left) and UV-Vis spectra (right), TAT-mAuNPs exhibited excellent stability during 24 h of incubation.

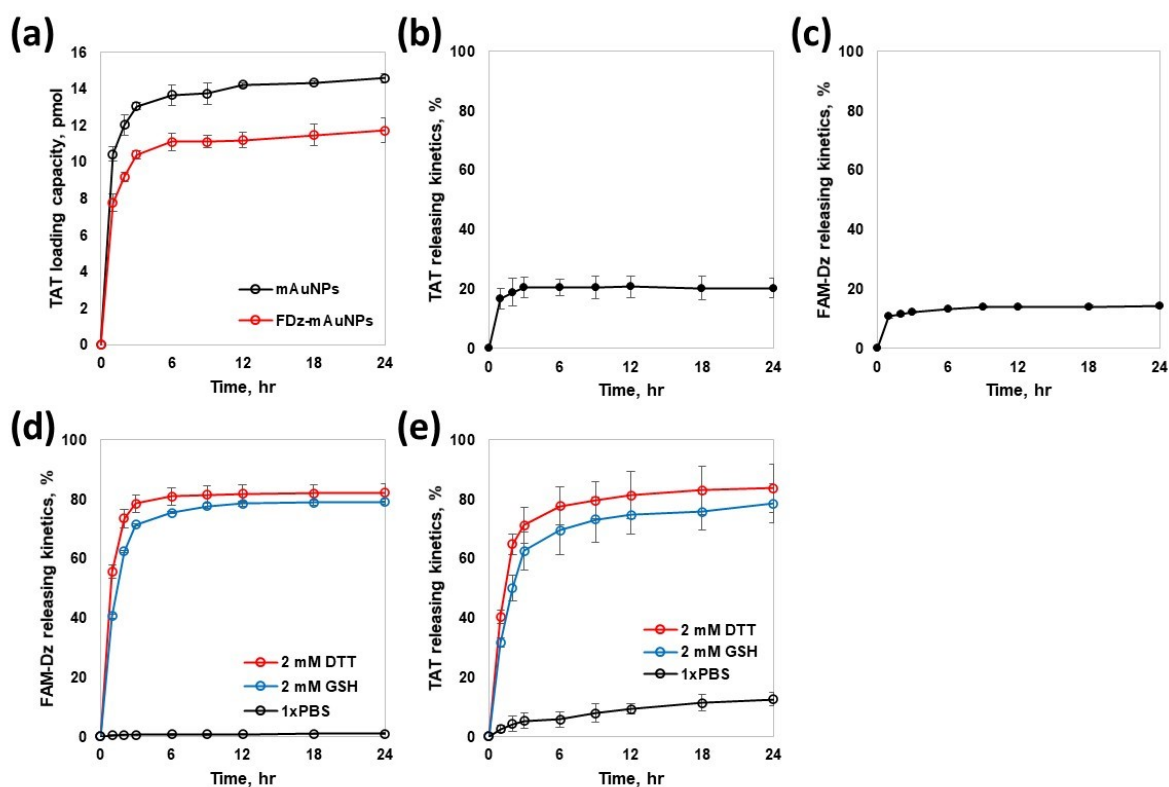


Figure S10. Loading and releasing profile of TAT and FDz against mAuNPs. (a) Loading capacity calculation of Cy5-TAT for mAuNPs and FDz-mAuNPs. Releasing of (b) TAT and (c) FDz from TAT-mAuNPs and FDz-mAuNPs respectively. TAT or FDz pre-loaded nanocomposites were incubated with opposite cargo to induce ligand exchange and subsequent releasing. (d) FDz releasing and (e) TAT releasing under the existence of DTT and GSH as Au-thiol bond exchange.

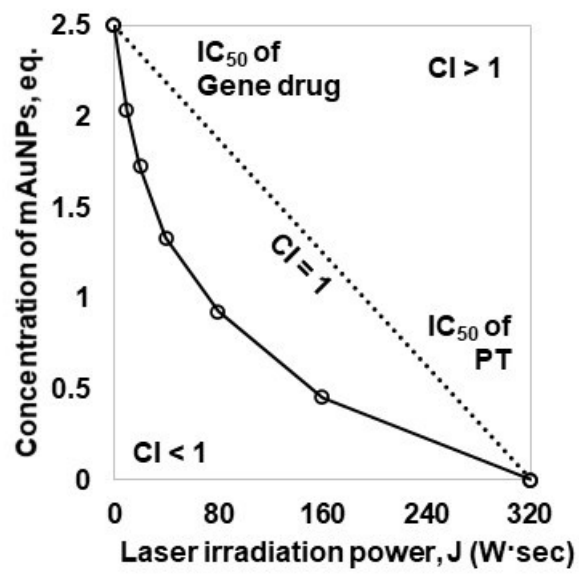


Figure S11. Gene delivery and PT synergistic effect isobologram.

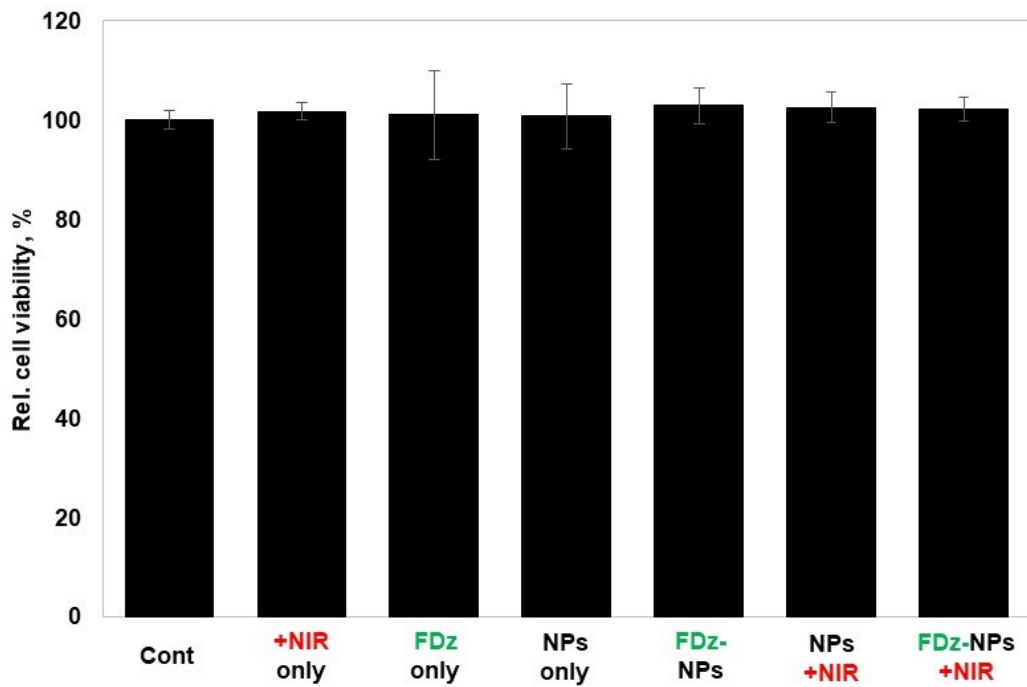
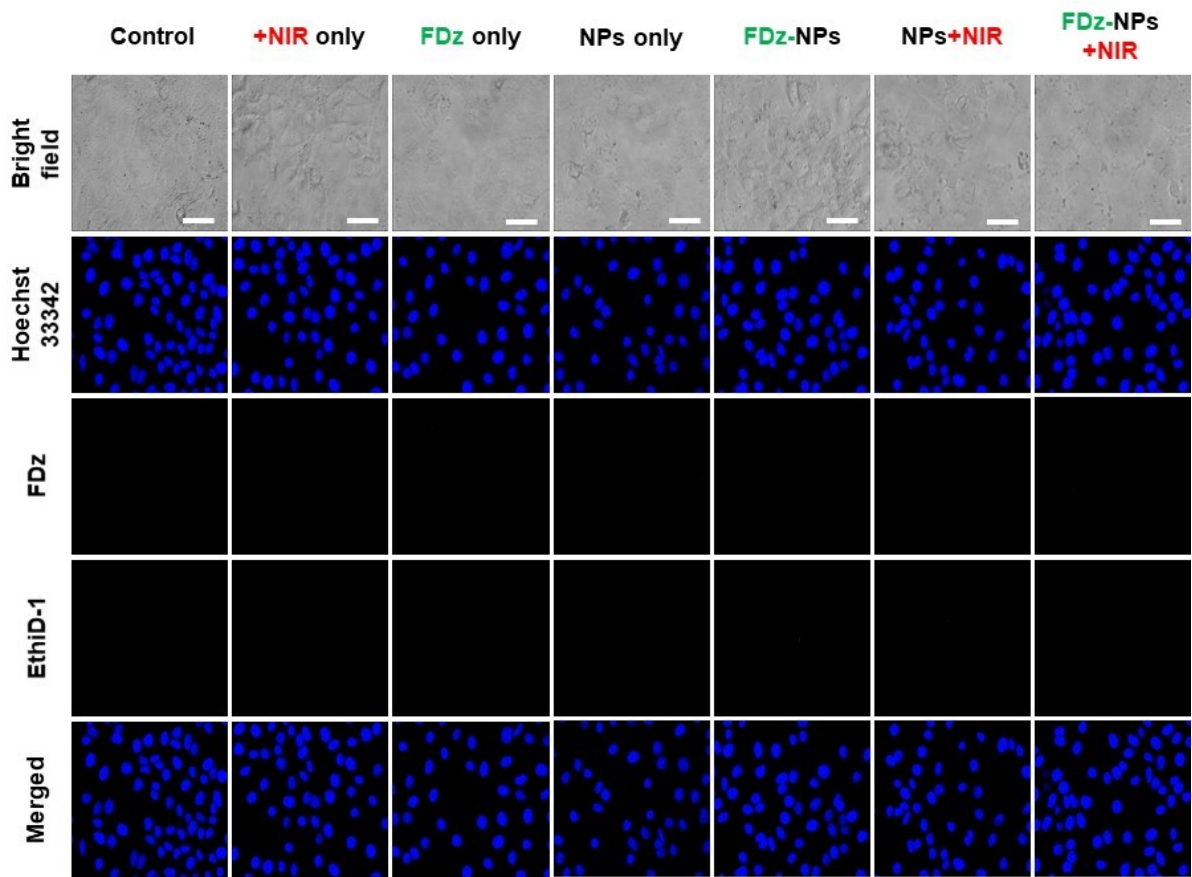


Figure S12. Gene-thermo cancer therapeutic efficacy by fluorescence microscope images (top) and relative cell viability (bottom). The scale bar is 50 μm .

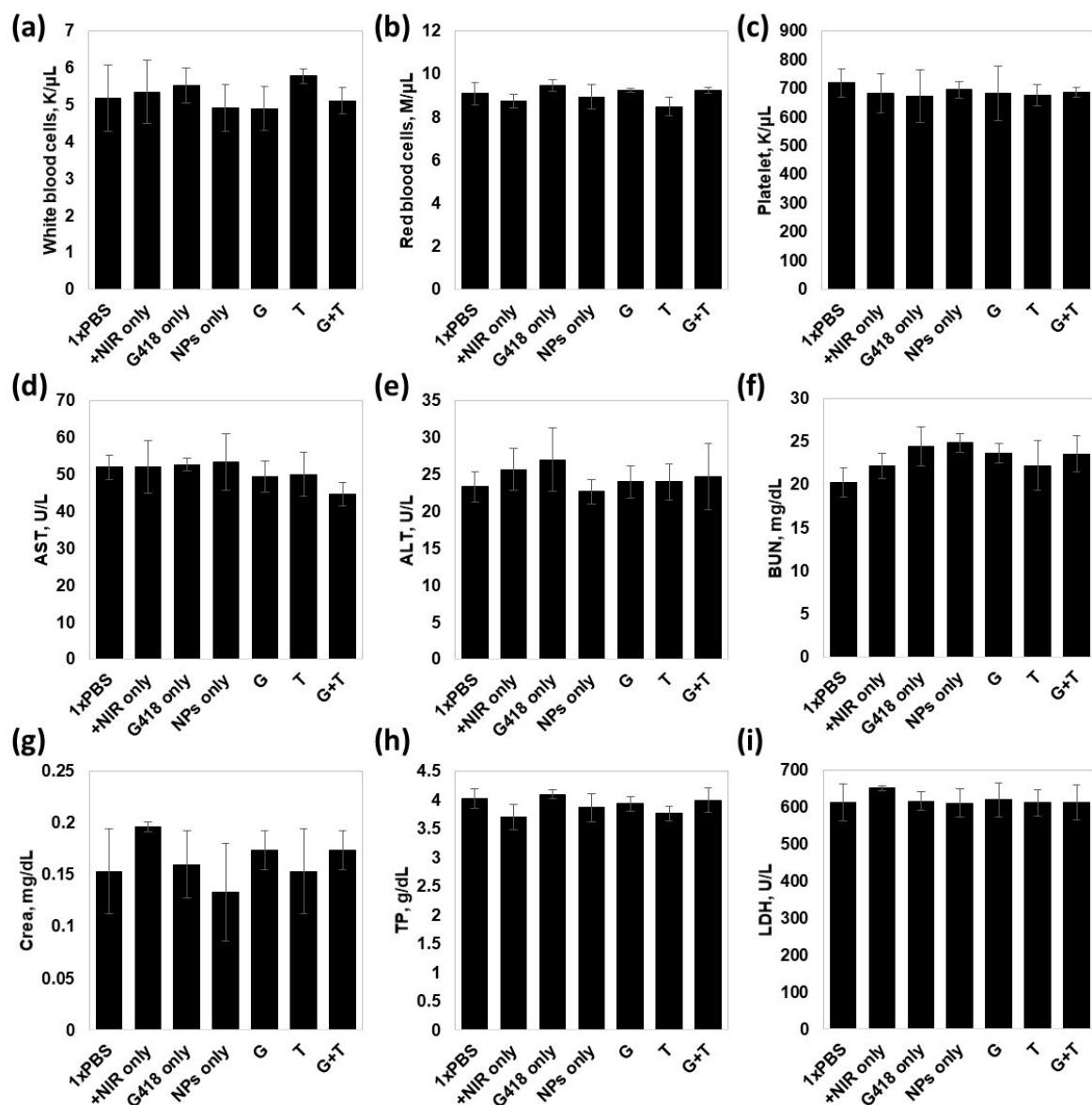


Figure S13. In vivo toxicity profile of TAT-mAuNPs by blood tests. (a-c) white blood cells, red blood cells, and platelets counts. (d,e) Hepatotoxicity profile by aspartate aminotransferase (AST) and alanine aminotransferase (ALT) expression level. (f,g) Renal toxicity profile by blood urea nitrogen (BUN) and creatinine (Crea) concentration. (h) Chronic toxicity identification by total protein and (i) cellular damage indicator lactate dehydrogenase level comparison.

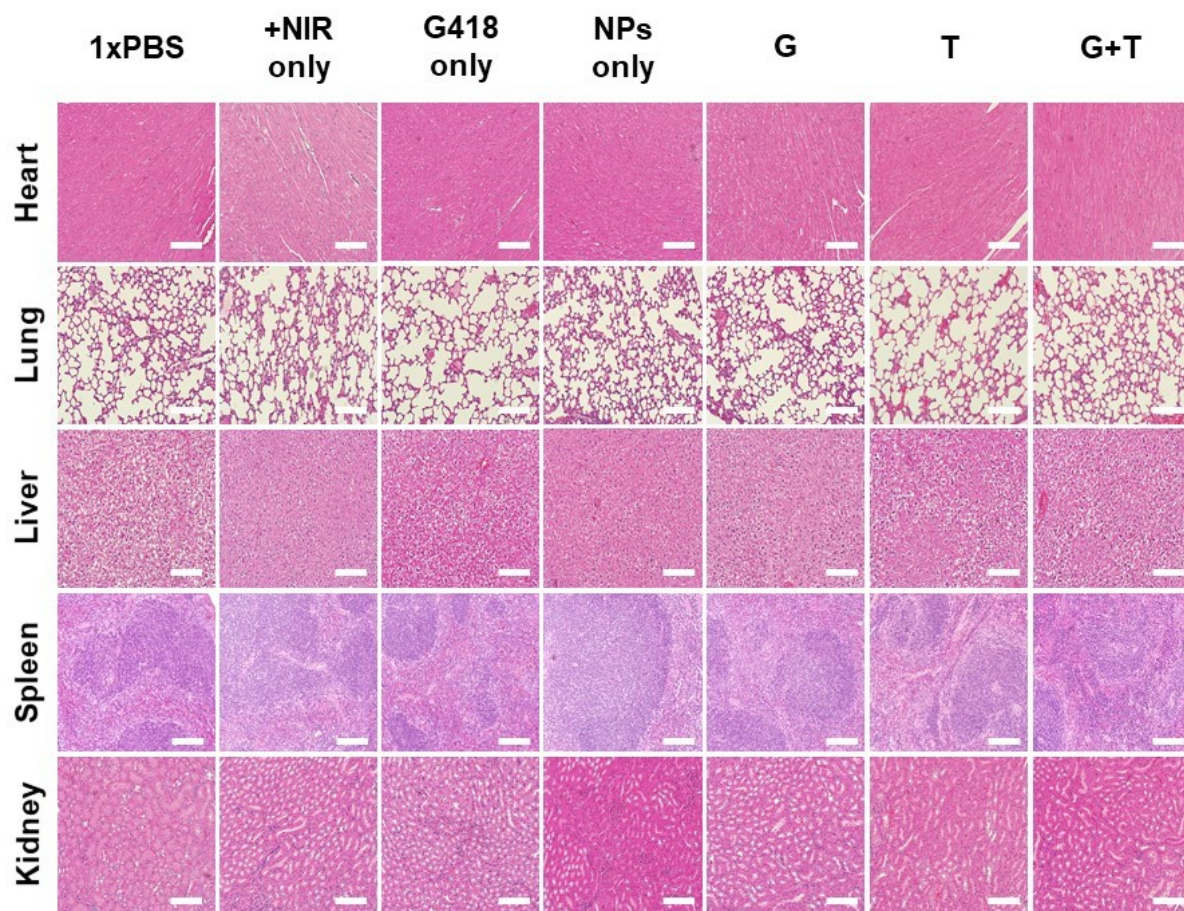


Figure S14. In vivo toxicity profile of TAT-mAuNPs by histological analysis for major organs.

The scale bar is 50 μm .